Chapter

Surface Measurement and Evaluation of Fiber Woven Composites

Bin Lin, Haoji Wang and Jinhua Wei

Abstract

The surfaces of fiber woven composites (FWCs), especially woven ceramic matrix composites (WCMCs), are obviously anisotropic. Many kinds of damage, which are different from traditional homogeneous materials, could be caused by the fabrication and machining process. The old surface evaluation system appropriate for isotropic materials is no longer suitable to WCMCs, thus causing many difficulties in terms of their wide industrial applications. This chapter presents a grading surface measurement and evaluation system for WCMCs based on their microstructures. The system includes four levels: fiber, fiber bundle, cell body, and the whole surface. On the fiber level, the typical forms of fiber damage, and their effects on the surface morphology of WCMCs are analyzed, which lays a foundation for the measurement and evaluation methods on the next three levels. On each subsequent level, the system proposes a set of surface measurement sampling parameter determination methods and surface quality evaluation methods based on the principle of statistics. As demonstrations, the surface measurement and evaluation on each level were processed on a carbon fiber-reinforced silicon carbide matrix composite (C_f/SiC) to illustrate the methodology of the system.

Keywords: woven ceramic matrix composites, grading surface evaluation, surface sampling method, confidence interval, residual error estimate

1. Introduction

Fiber woven composites (FWCs) are a kind of new fiber composites. The fibers inside are woven to form a preform, and then the matrix grows on the preform to generate the final composites. The woven fibers can heighten the reinforcing effect of the fibers and improve the mechanical property of the composite. Therefore, FWCs could perform better than other fiber composites.

Among FWCs, woven ceramic matrix composites (WCMCs) are star materials, widely used in aerospace, military, national defense, and some other advanced fields [1–4], because of their high specific strength and rigidity, corrosion and wear resistance, and other excellent characteristics [5, 6]. For the industrial application of WCMCs, it is of vital importance to objectively evaluate the surface processing quality and, on this basis, judge the type and degree of processing damage. To do so, it is essential to measure the surface topography both accurately and efficiently and select proper indexes to evaluate the surface process quality. However, WCMCs are

far more complicated than traditional materials. On the one hand, their surfaces are anisotropic and inhomogeneous and have obvious directionality and complex structures, which means that there are difficulties and challenges in measuring and evaluating their surfaces. Traditional surface measurement and evaluation approaches for isotropic materials are no longer suitable to WCMCs [7–9]. On the other hand, the surfaces of an WCMC present more types of processing damage than isotropic materials, including fiber pullout, debonding, and matrix cracking [10]. Each shows a different influence on the composite application, and thus judging the type and degree of processing damage to a WCMC is a new but difficult task.

To date, there have been no uniform measurement standards to ensure that undistorted WCMC surface features are obtained or proper evaluation approaches accurately assess the surface damage [11, 12]. It is widely believed that only 3D measurements can obtain the complete surface information [7, 13, 14]. However, a traditional evaluation method used to assess the isotropic materials is limited to a quantitative description of the entire surface through some typical surface topography parameters, which ignores the subtle details of the surface. Such judgment standards are brief with respect to the direct relation to the surface damage. Moreover, to date, a majority of composite surface evaluations still use the profile arithmetic mean error *Ra* as the only evaluation parameter [15–20], which is fairly incomplete.

As such, the complexity of a WCMC surface calls for a newer and more targeted methodology that is tightly connected with the topography characteristic. When we look into the WCMC surface, it is obvious that its composition sequence is as follows: fiber -fiber bundle -cell body -whole surface [21]. Here, a fiber is the smallest composing unit, a fiber bundle is the smallest structural unit, and a cell body is the smallest repeatable unit. A cell body is made up of fiber bundles and matrix and has a nearly fixed surface microstructure. The material surface is formed through its repeating copy and translation [22, 23]. Thus, fiber damage influences the fiber bundle surface, damage to the fiber bundle surface influences the cell body surface, and damage to the cell body surface influences the whole surface property. Merely depicting the entire surface at one time without considering the surface structure composition of a WCMC is inadvisable.

In this chapter, it is proposed that the measurement and evaluation of a WCMC surface should adopt a grading evaluation system based on its complex surface structure, which includes the four levels: fiber, fiber bundle, cell body, and the whole surface. On the fiber level, the typical forms of fiber damage and their effects on the surface morphology of WCMCs are analyzed, which lays a foundation for the measurement and evaluation methods on the next three levels. On each subsequent level, the system proposes a set of surface measurement sampling parameter determination methods and surface quality evaluation methods based on the principle of statistics.

2. Fundamental concepts, devices, and materials of the research

2.1 The microstructure of a WCMC surface

According to the common fabrication process of WCMCs (shown in **Figure 1**), single fibers are surface modified to improve the bonding strength between fibers and matrix, and then several fibers are twined to form a fiber bundle. Multiple fiber bundles are woven in a certain way to a preform. The preform is then immersed

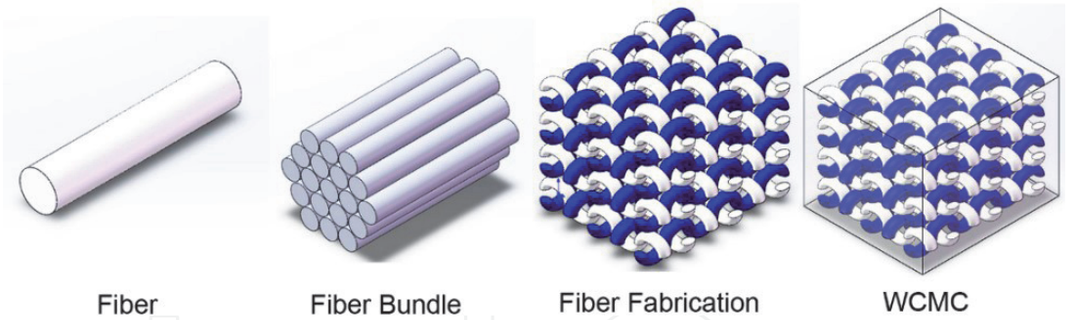

Figure 1.
The fabrication process of an WCMC.

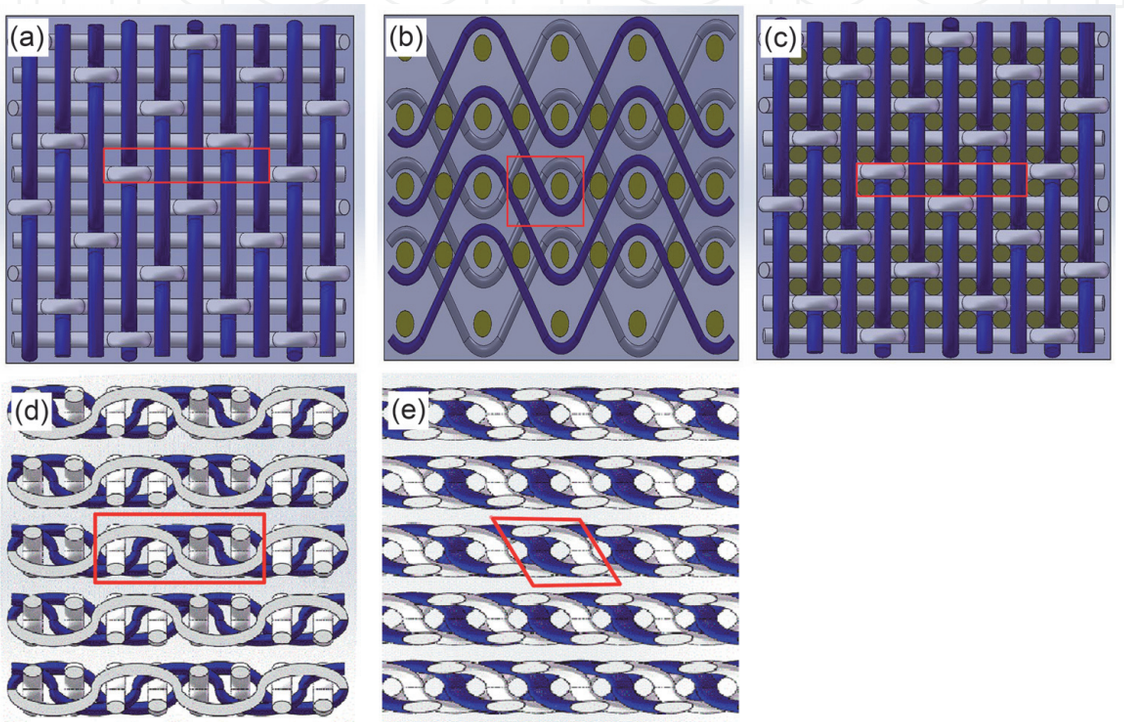

Figure 2.
Schematic diagram of different woven patterns of WCMC. (a) 2D, (b) 2.5D, (c) 3D, and (d) 2D woven style with a processing angle of 90° and (e) 2D woven style with a processing angle of 45°.

into an environment with the elements or components of the matrix. The matrix can grow on the preform to generate the final WCMCs.

The schematics of the WCMC surfaces of different woven methods (shown in **Figure 2(a–c)**) and process angles (shown in **Figure 2(d, e)**) indicate that there exists a minimum repeatable unit, which is marked with a red block in the figures. The unit is composed of the fiber bundles of every directions and the ceramic matrix. The whole surface can be formed through its repeating copy and translation. The unit is defined as the "cell body" in this chapter. It is obvious that the shape of a cell body is not uniform for a WCMC. In fact, the appearance of a cell body can change with different woven methods and process angles.

In summary, fiber is the minimum characteristic of a WCMC, which forms fiber bundle. Fiber bundles are woven to different directions. The cell body consists of fiber bundles of every directions and the matrix. Eventually, the whole surface is generated by copy and translation of the cell body. Therefore, fiber is the minimum evaluable unit of WCMCs. Its damage form can influence the surface state of fiber bundles. Fiber bundles build a bridge between the "microscale" of the fiber and the

"macroscale" of the cell body. Their surfaces include the information of the fibers and impact the surface quality of the cell body. Cell body is a key feature. On the one hand, its components are as complicated as the whole surface, which means that the evaluation results of a cell body can be used to represent and estimate a certain range of a whole surface. On the other hand, it is obviously affected by the fiber bundles and matrix inside; thus the analysis of fiber and fiber bundle can be used to evaluate the cell body.

In this chapter, it is believed that the measurement and evaluation of WCMCs should employ a grading system. The evaluation of fiber, fiber bundle, cell body, and the whole surface should be separately researched and then integrated. On the fiber level, the typical damage forms of fibers should be identified and classified, and how the damage influence the using properties should be research. On the subsequent levels, two tasks should be accomplished. The first one is to select proper sampling methods to acquire the undistorted surface information. And the second one is to propose and test reliable evaluation indexes to quantitatively estimate the main damage type and degree of the surfaces. With all the work above, a grading measurement and evaluation system for the surface of a WCMC can be eventually built. The following parts of this chapter introduce the methodologies on each level.

2.2 The effect of fiber damage on the surface measurement and evaluation of WCMCs

When processed by machining tools, the surfaces of WCMCs interact with the cutting edges, leading to fiber damage. The damage of fiber on the one hand causes the removal of fibers and, on the other hand, turns into the machining defects on the surfaces. The multifarious types of the damage of WCMCs are the main feature of difference to the traditional homogeneous materials and, meanwhile, are the main source of technological difficulty of the evaluation of WCMCs.

The typical forms of damage on the surfaces of WCMCs are the following:

Fiber fracture, which is caused by the cutting edges directly cutting the fibers off, often happens when the fibers at the cutting area are tightly fixed by the matrix or by other fibers nearby. The cutting section of fiber fracture is V-shape, and the bottom of the V often appears plastic deformation, which is caused by the friction and squeezing between the fibers and the cutting edges. Fiber fracture is the most common material removal form of WCMCs. If the materials are mainly removed by fiber fracture, the finished surfaces are always of good quality and with low roughness.

Fiber pulled-off is caused by the cutting edges breaking the matrix without cutting off the fibers or the cutting edges pulling the fibers out of matrix without cutting them off. This type of damage can leave fibers exposed or form holes on the finished surface, which decreases the surface quality. When the finished surface is assembled with another part, the raised fiber can act as a tiny cutting edge, harming the counterpart surface. When the finished surface performs as a friction surface, the holes may help contain lubricating oil and wear debris, alleviating three-body wear, thus improving its tribological performances.

Fiber debonding, which is caused by the cutting edges removing the entire layer of fibers, often occurs when the fibers at cutting area are poorly connected with the matrix. Fiber debonding can result in collapses of large areas on the surface and greatly reduce the surface quality.

From the analysis above, it is clear that the machining process can cause manifold types of damage on the surface of WCMCs. Each kind of damage can affect the quality and performance of the surface in its own way. Therefore, the evaluation

technology of WCMCs is required to recognize the main type of damage on a surface and quantitatively estimate the degree of the damage.

Moreover, fiber bundles, cell bodies, and the whole surface are, basically speaking, made up of fibers. Because of the directional arrangements of fibers, the height of the surface of WCMCs could fluctuate with the period of fiber diameter. The fiber diameter acts as an obvious fundamental frequency on the surface of WCMCs. It can influence the sampling parameters, such as sampling step, sampling length, and sampling area, on other levels. Meanwhile, the direction of fibers determines the direction of the fundamental frequency and can eventually influence the sampling direction. Thus, the direction and diameter of fibers are tightly connected with the surface measurement technology of WCMCs.

In conclusion, fiber, as the minimum evaluable unit of a WCMC surface, significantly influences the grading surface measurement and evaluation system of WCMCs. On the one hand, when considering whether an evaluation index is appropriate for WCMC surface, it should be checked whether this index can help recognize and estimate the type and degree of damage. On the other hand, when determining the proper sampling parameters, the directionality and the diameter of fibers must be taken into consideration.

2.3 Surface measurement technology and devices

The measurement of a surface is a process that obtains the height information of the surface. Surface measurement methods are divided into two classes: contact measurement, which uses a probe to measure the height data of points on the surface, and non-contact measurement, which uses light to measure. It was always believed that contact measurement could achieve higher measurement accuracy, although its efficiency was quite low and the measurement process was time-consuming. However, thanks to the development of optical theories and technologies, the non-contact measurement technology based on white light interferometry can get extremely high level of accuracy now as well. NANOVEA ST400 (shown in **Figure 3**), an optical non-contact measurement system, is used to measure the surface micro-topography in the research of this chapter.

Because the measurement of a surface is in fact the measurement of the points on the surface, it has to be determined which points are chosen to be measured. This

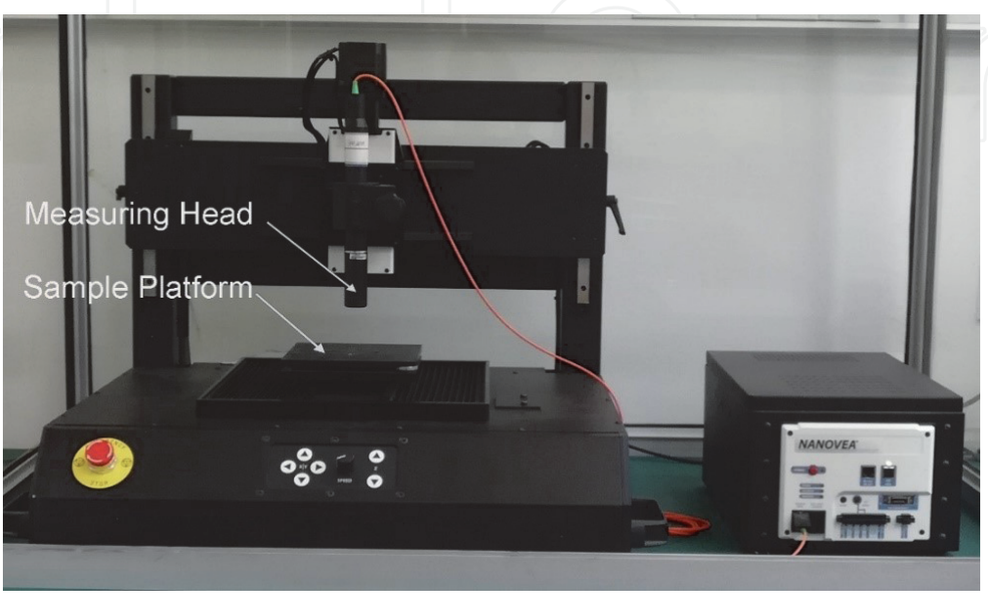

Figure 3.
Three-dimensional non-contact surface morphometer.

topic is related to the sampling strategy, which means how to choose a proper set of points to measure, in order to make the measurement results of these samples able to reflect the information of the entire surface. The first question is to use 2D measurement or 3D measurement.

If a 2D measurement is adopted, points in a line are measured and calculated as one data set. In this term, sampling step (the length between two adjacent sampled points), sampling length (the length of the entire sampling line), and sampling direction (the angle between the sampling line and the structure of the surface) should be determined. In most instances of 2D measurement, one line of sampling is not able to reflect the entire surface because of the measuring error and the random surface damage. Several lines should be selected and measured in order to improve the stability of the measurement results. Therefore, sampling number (the number of the sampling lines) is also to be determined.

If a 3D measurement is adopted, an array of points inside the entire surface are measured and calculated as one data set. That's to say, the sampling area is the area of the entire surface. When sampling step is determined, the points to be measured are selected. It was believed that 3D measurement was more adaptable for complex surfaces because it could get more information of the surfaces. However, the research of this chapter proved that, if the surface to be measured is obviously directional, 3D measurement will lose its advantages and 2D measurement should be adopted. On the other side, 3D measurement always means long sampling time, huge data processing work, and, thus, low efficiency.

Selecting proper sampling parameters, including sampling step, length, direction, number of 2D measurement, and sampling step of 3D measurement, is a complex work. Small step and large length and number are always related to higher measuring accuracy but low efficiency and vice versa. Proper sampling parameters balance both two sides, maintain undistorted sampling, and, on this basis, reduce sampling points.

2.4 Surface evaluation technology

The task of surface evaluation technology is to select proper statistical characteristics (defined as evaluation indexes in this chapter), which can be calculated from the measurement data of the heights of the sampling points. The following are the indexes adopted in the research of the chapter:

For 2D measurement data:

For each sampling profile j, its average is defined as μ_{0j}, the standard deviation is σ_{0j}, and the normalized height of every sampling point is Z_{0ij}, and thus

$$\mu_{0j} = \sum_{i=1}^{M} Z_{ij}/M \tag{1}$$

$$\sigma_{0j} = \sqrt{\sum_{i=1}^{M} \left(Z_{ij} - \mu_{0j}\right)^2/(M-1)} \tag{2}$$

$$Z_{0ij} = \left(Z_{ij} - \mu_{0j}\right)/\sigma_{0j} \tag{3}$$

where the height of every sampling point is defined as Z_{ij}, j is the jth profile on the fiber bundle surface, and the number of sampling points within the sampling profile is M, where M = the *sampling length*/*sampling step*.

Based on the above, the four 2D evaluation indexes used in the chapter are profile arithmetic mean error *Ra*, profile square root deviation *Rq*, profile skewness *Rsk*, and profile kurtosis *Rku*, which can be calculated as follows:

$$Ra_j = \sum_{i=1}^{M} |Z_{ij}| / M \tag{4}$$

$$Rq_j = \sqrt{\sum\nolimits_{i=1}^{M} {Z_{ij}}^2 / M} \tag{5}$$

Here, *Ra* and *Rq* are quite similar in reflecting the surface roughness, although *Rq* is in general more sensitive than *Ra* to the degree of surface roughness.

The normalized R_{sk0} and R_{ku0} of the *j*th profile can be obtained as follows:

$$Rq_{0j} = \sqrt{\sum\nolimits_{i=1}^{M} {Z_{0ij}}^2 / M} \tag{6}$$

$$Rsk_{0j} = \sum_{i=1}^{M} {Z_{0ij}}^3 / \left(M {Rq_{0j}}^3 \right) \tag{7}$$

$$Rku_{0j} = \sum_{i=1}^{M} {Z_{0ij}}^4 / \left(M {Rq_{0j}}^4 \right) \tag{8}$$

According to the definition of *Rsk*, the closer it is to 0, the more approximate the sampling profile is to a Gaussian distribution. When $Rsk > 0$, the profile presents a positive peak. This indicates that the profile has more crests or the crest height is larger than the trough height. In contrast, if a profile has more troughs, or the trough height is larger than the crest height, it presents a negative peak.

On the other hand, *Rku* is compared with 3. The closer it is to 3, the more approximate the sampling profile is to a Gaussian distribution. That is, the degree of dispersion of the profile data is similar to a Gaussian distribution profile. The more *Rku* is greater than 3, the smaller the degree of data dispersion is, and in contrast, the more *Rku* is less than 3, the larger the degree of data dispersion is.

For 3D measurement data:

The four 3D evaluation indexes used in the chapter are surface arithmetic mean deviation *Sa*, surface square root deviation *Sq*, surface skewness *Ssk*, and surface kurtosis *Sku*, which can be calculated as follows:

$$Sa = \sum_{i=1}^{M} \sum_{j=1}^{N} |Z_{ij}| / M / \mathrm{N} \tag{9}$$

$$Sq = \sqrt{\sum\nolimits_{i=1}^{M} \sum\nolimits_{j=1}^{N} {Z_{ij}}^2 / M / \mathrm{N}} \tag{10}$$

$$Ssk = \sum_{i=1}^{M} \sum_{j=1}^{N} {Z_{ij}}^3 / \left(MN {Sq}^3 \right) \tag{11}$$

$$Sku = \sum_{i=1}^{M} \sum_{j=1}^{N} {Z_{ij}}^4 / \left(MN {Sq}^4 \right) \tag{12}$$

where the height of every sampling point is defined as Z_{ij} and the number of sampling points within the sampling area is *M* and *N*, where *M* and *N* = the *sampling length* (of X and Y direction, respectively)/*sampling step*.

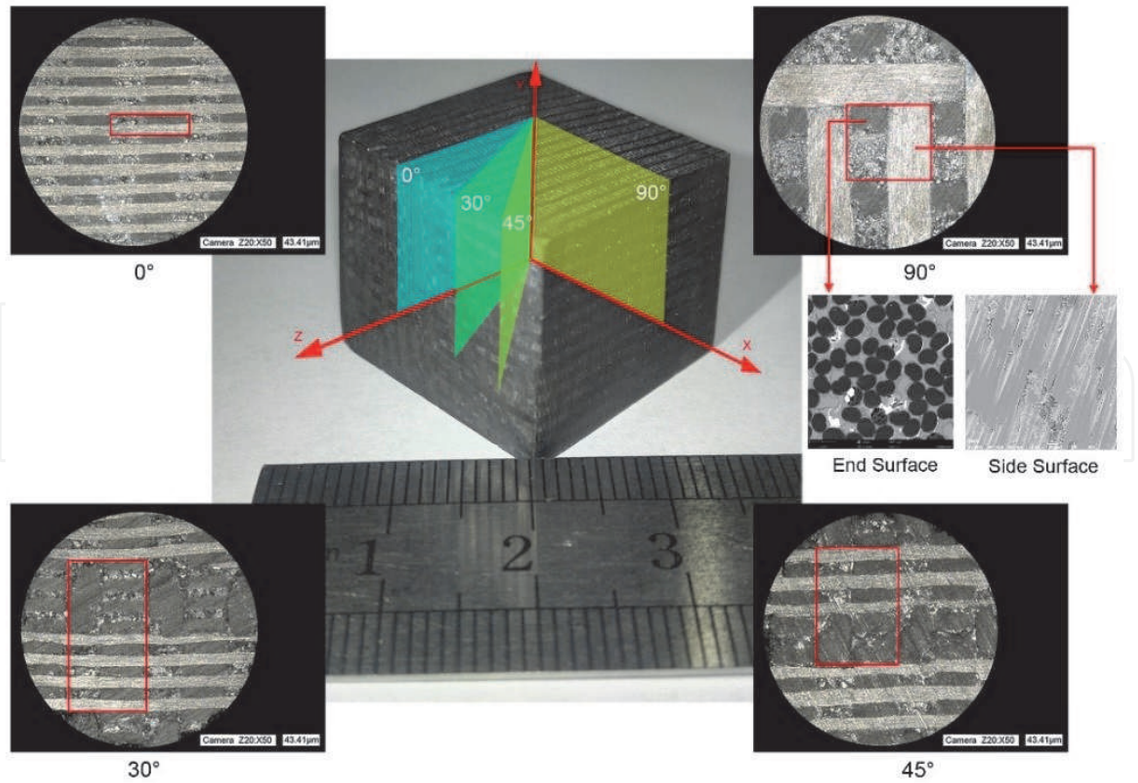

Figure 4.
Definition of the processing angle of C_f/SiC [26].

2.5 Materials used as examples in the chapter

In order to illustrate the measurement and evaluation method, several materials were measured and evaluated as examples in this chapter. The information of the materials is shown as follows:

The carbon fiber-reinforced silicon carbide ceramic matrix composite (C_f/SiC) was fabricated through chemical vapor infiltration (CVI) combined with a liquid melt infiltration process (LMI) [24]. The preform was prepared using a 3D needling method and densified using CVI to form a porous carbon/carbon (C/C) composite. Next, the porous C/C composite was converted into C_f/SiC during LMI, in which silicon carbide (SiC) matrix was formed through a reaction with carbon and melted silicon [25]. The density of the C_f/SiC composite is 1.85 g/cm^3.

The fiber diameter of the material is about 7 μm, and size of the cell body is about 1.6 mm × 1.6 mm.

The C_f/SiC specimens were ground with four different processing angles. For 90° processing angle, the fiber bundles are divided into side fiber bundles and end fiber bundles, according to their directions (shown in **Figure 4**).

3. The measurement and evaluation of fiber bundle surfaces

3.1 Measurement strategy and sampling direction

When measuring fiber bundle surfaces, 2D measurement should be adopted because of the obvious directionality of the surfaces. Here we take the surface of C_f/SiC with a processing angle of 90° as an example. Owing to the directionality of the fiber bundles, different sampling directions often result in different numerical characteristics, as shown in **Figures 5** and **6**. We can see that no matter what type of measurement direction is applied, there is no influence on the 3D surface

topography. That is, a 3D sampling and evaluation method may not be able to reflect the surface details of the fiber bundle. The use of one or a group of 3D evaluation indexes based on a 3D sampled data fails to reflect the damage types related to the fiber orientation and machining direction.

On the side surface of a fiber bundle, the bonding strength between the fiber and matrix is weaker than that of the end surface. The most direct reflection of the machining direction is fiber damage such as fiber debonding, fiber fractures and delamination. The fiber direction scale is more notable than the machining direction scale, and the directionality of the surface topography mainly depends on the fiber orientation. On the end surface of a fiber bundle, the fiber is mainly subjected to a shear force. The main fiber damage is fiber shearing and fiber pullout. The machining

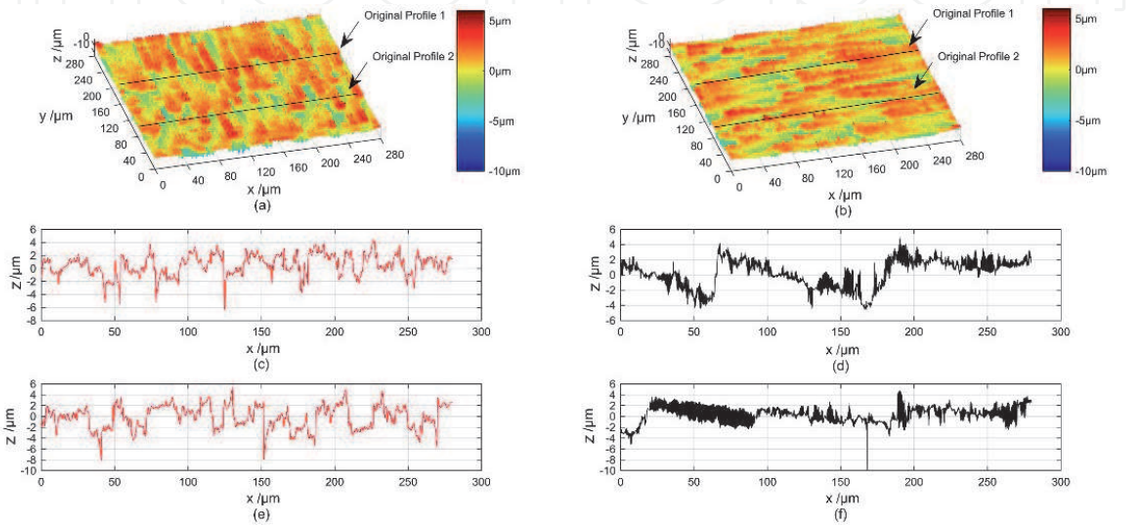

Figure 5.
Side surface topography of a fiber bundle with a scanning track perpendicular and parallel to the fiber direction [27]. (a) Surface topography-scanning track perpendicular to the fiber direction. (b) Surface topography-scanning track parallel to the fiber direction. (c) Original profile 1, scanning track perpendicular to the fiber direction. (d) Original profile 1, scanning track parallel to the fiber direction. (e) Original profile 2, scanning track perpendicular to the fiber direction. (f) Original profile 2, scanning track parallel to the fiber direction.

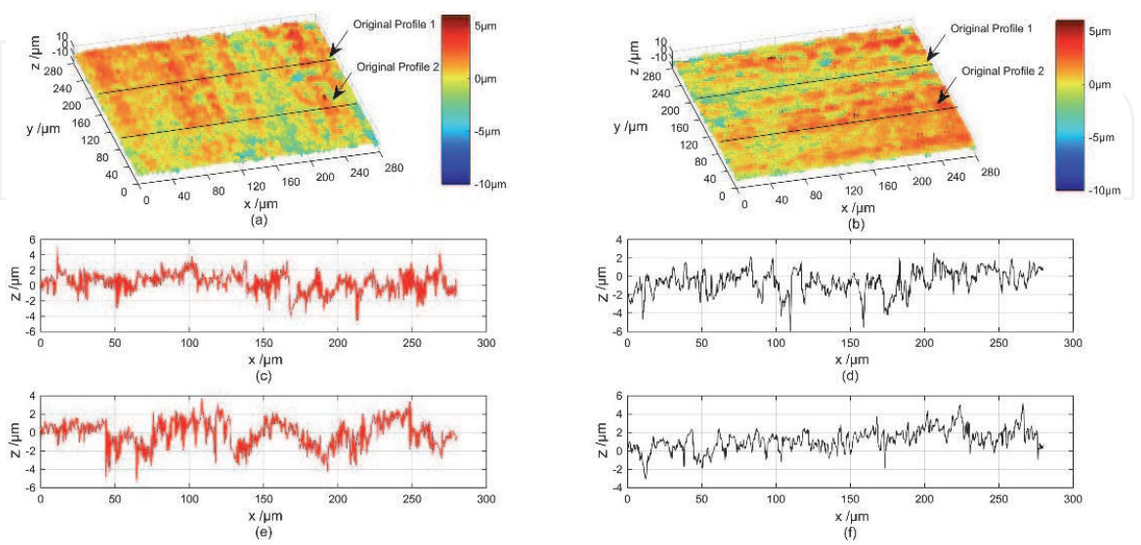

Figure 6.
End surface topography of a fiber bundle with a scanning track perpendicular and parallel to the machining direction [27]. (a) Surface topography-scanning track perpendicular to the machining direction. (b) Surface topography-scanning track parallel to the machining direction. (c) Original profile 1, scanning track perpendicular to the machining direction. (d) Original profile 1, scanning track parallel to the machining direction. (e) Original profile 2, scanning track perpendicular to the machining direction. (f) Original profile 2, scanning track parallel to the machining direction.

direction scale is more notable than the fiber orientation scale, and the directionality of the surface topography mainly depends on the machining direction.

On the side surface of a fiber bundle, as shown in **Figure 5(c, e)**, when the scanning track is perpendicular to the fiber direction, the profile shows damage between fibers, whereas the profiles only show single fiber damage when the scanning track is parallel to the fiber direction (**Figure 5(d, f)**), which means that the profiles cannot reflect the machining effect on the whole fiber bundle surface. The same phenomenon occurs in the end surface of a fiber bundle. When the scanning track is perpendicular to the machining direction, the profile shows the integrated influence of the processing (**Figure 6(c, e)**); however, when the scanning track is parallel to the machining direction, the profiles simply show the effect of a single grain on the surface (**Figure 6(d, f)**).

From the analysis above, it can be seen that the 2D sampling and evaluation method is more suitable for a fiber bundle scale measurement. To guarantee measurement accuracy and consider the influence of the fiber orientation and machining direction on the surface topography, the scanning track should be perpendicular to the fiber orientation on the side surface of a fiber bundle and perpendicular to the machining direction on the end surface.

According to our research, it may be reasonably inferred that, for planes which are not truly along the fibers, the influence of the fiber orientation and machining direction should be considered. When the surface is full of processing traces and the fiber orientation is so obscure, the sampling direction should be perpendicular to the machining direction. In other cases, the sampling direction should still be perpendicular to the projection direction on the vertical plane along the fiber axis. However, a definite conclusion in this regard still requires further research.

3.2 Determination of sampling length and number

The side surface of C_f/SiC with processing angle of 90° is taken as an example to illustrate the determination method of sampling length when measuring a fiber bundle surface. Since the diameters of the fibers are approximately 7 μm, a set of candidate sampling length are chosen as the integral multiple of 7 μm, namely, 7, 14, 21, 28, 35, 42, 49, 56, 63, 70, 77, 84, 91, 98, 105, 112, 119, 126, 133, 140, and 147 μm. In each sampling length, 1500 surface profiles are measured with a constant sampling step of 0.1 μm. And 2D surface roughness *Ra* of each profile is obtained.

According to the numerical values of 1500 *Ra*, a frequency histogram is made. It can be seen that the distribution of 2D surface roughness *Ra* in every sampling length is almost of its normal distribution. The result shown in **Figure 7** is the one using normal distribution function to fit the frequency histogram. With the growth of sampling length (**Figure 8(a)**), the curves are thinner and higher. Their shapes do not change any more in the case that sampling length is more than a certain value (**Figure 8(b)**). It is known to all that normal distribution has two parameters: the mean value μ and the standard deviation σ. μ is the location parameter and describes the central tendency position of the normal distribution. σ demonstrates the discrete degree of data. The larger the σ is, the more decentralized the data is, leading to a fact that the curve is fatter and lower. On the contrary, the more concentrated the data is, the thinner and taller is the curve. That is to say, *Ra* is gradually convergent and concentrated while the sampling length increases.

Figure 8 clearly shows the changing trends of standard deviation σ and the mean value Ra_{ave} of 1500 2D surface roughness *Ra* under different sampling length. It can be found that with the increase of sampling length, both σ and Ra_{ave} are gradually

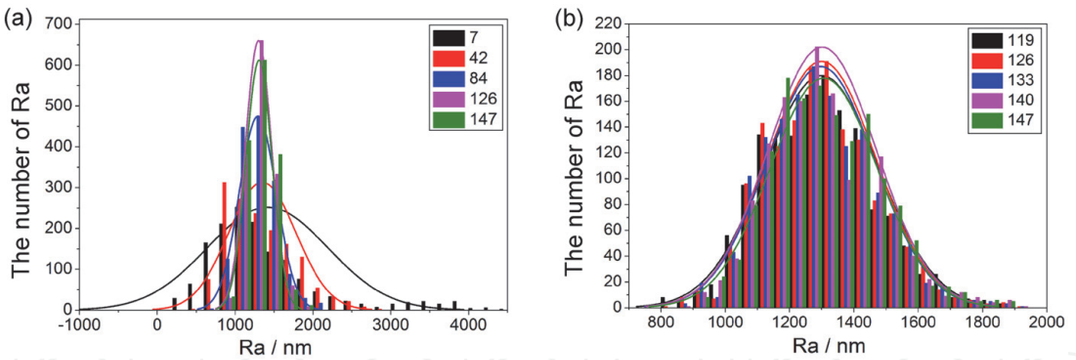

Figure 7.
The distribution of 2D surface roughness Ra under different sampling length [24]. (a) With the sampling lengths of 7,42 84 125 and 147. (b) With the sampling lengths of 119,126 133 140 and 147.

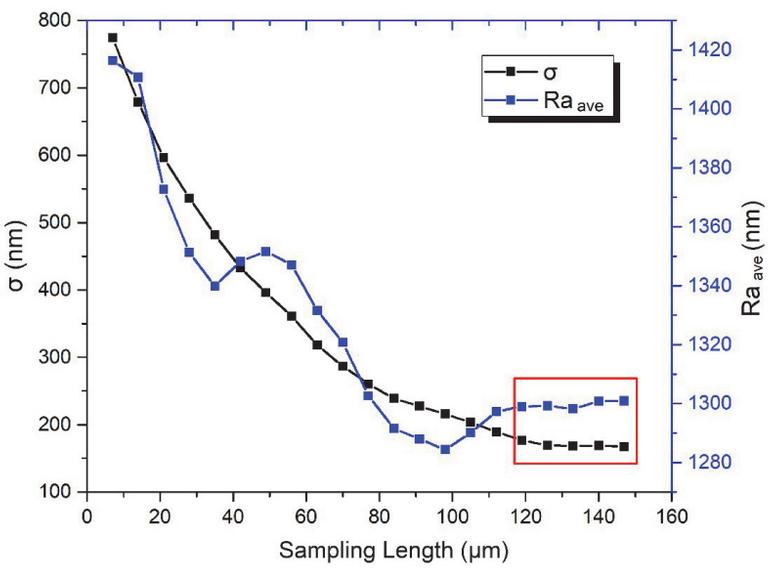

Figure 8.
The changing trends of σ and Ra_{ave} under different sampling length [24].

decreasing and becoming steady. When the sampling length reaches to 120 μm, Ra_{ave} is stable around 1297.3 nm.

Based on the results obtained above, a speculation is proposed that the mean value of a few number of *Ra* can steadily estimate the entire surface roughness of fiber bundle. The average value of *Ra* under the changing sampling number from 10 to 150 and the constant sampling length 120 μm could be obtained, which is represented by Ra_{avg}. Under every sampling number, the measurement process repeats 50 times independently. Then the maximum relative error of every sampling number, calculated by Eq. (13), is demonstrated in **Figure 9**. It is shown that with the rise of sampling numbers, the maximum relative error would decrease dramatically. Once the number of *Ra* reaches to 70 or above, it is stable under 2%, which is acceptable in terms of accuracy.

$$\delta = \left|Ra_{ave} - Ra_{avg}\right| / Ra_{ave} * 100\% \tag{13}$$

According to the analysis given above, the conclusion can be made that as long as extracting surface profiles averagely distributed on the side surface of C_f/SiC composite fiber bundle with the appropriate sampling length and sampling number, the mean value of Ra is steady and can estimate the whole surface roughness. For

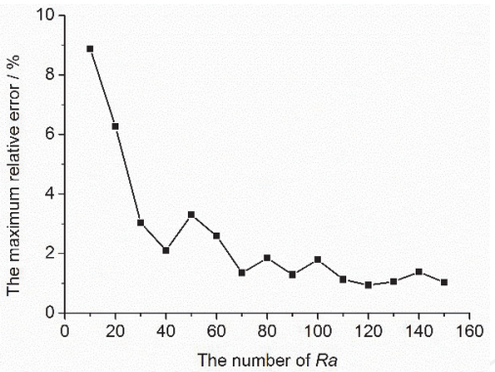

Figure 9.
The changing trend of the maximum relative error under different number of Ra [24].

C_f/SiC composite used in the present work, the critical sampling length is 119 μm, which is about 17 times of the fiber diameter, and sampling number is 70.

3.3 Determination of sampling step

In this section, the side surface and end surface of C_f/SiC with processing angle of 90° are taken as an example to illustrate the determination method of sampling step, under the condition that the critical sampling length is 150 μm and sampling number is 200. It is clear that using a smaller sampling step can achieve more accurate surface data, whereas a too small step may cause an unnecessary sampling time and data processing cost. A method is proposed to determine the maximum sampling step (MaxSS) that can minimize the data size under the premise of undistorted surface sampling.

We start from setting the data measured at the step of 0.05 μm as a certain type of real value μ of surface topography parameters. The data measured using larger steps are to be compared with the real values μ to determine whether they are acceptable in terms of accuracy. To set a range of acceptance, the idea of a confidence interval in probability theory is used. If the real value is μ, a measurement result that is acceptable based on confidence level of 1-α must fall into a computable interval. Based on the probability theory, when the mean value of the overall sample μ is known and the standard deviation σ is unknown, the confidence interval of the mean value μ with the confidence level $(1-\alpha)$ is

$$\left[\mu - t_{\alpha/2}(n-1)S/\sqrt{n}, \mu + t_{\alpha/2}(n-1)S/\sqrt{n}\right] \tag{14}$$

where S is the standard deviation of the samples and n is the number of the samples.

By looking up the table-α quantile of the t-distribution, $t_{\alpha/2}(n-1)$ is available, and thus the corresponding confidence intervals are obtained. Therefore, the sampling step gradually increases until the measurement result falls out of the acceptance range at that step. This means that this step, and the steps larger than it, can no longer achieve accurate surface data. The largest permitted sampling step can be determined under each single evaluation index. Combining all indexes, the global MaxSS can be determined.

Here, Ra_{ave}, Rq_{ave}, Rsk_{ave}, and Rku_{ave} on a Cf/SiC fiber bundle surface are taken as the evaluation standards. For each index, the real value is determined as the value measured based on a sampling length of 150 μm, sampling number of 200, and sampling step of 0.05 μm. In addition, $t_{\alpha/2}(n-1)$ can be found to be 2.326 when the confidence coefficient is 98%. After that, μ and S can easily be calculated. The

acceptance range of each index is obtained through Eq. (14). The sampling length and sampling number are invariable, and the sampling step is gradually increased. All measurement results are shown in **Figure 10** (side surface) and **Figure 11** (end surface).

What needs to be mentioned is that the data used in **Figures 10** and **11** are acquired using a sampling direction perpendicular to the fiber orientation on the side surface and the machining direction on the end surface. For each index, the upper and lower limits express the acceptance range. The measurement result that first falls out of range is marked with a red box, and the last sampling step before it is the MaxSS of this index. Combining all four indexes on each surface, the global MaxSS is 0.75 μm on a side surface and 1 μm on an end surface, which are approximately 1/10 of the fiber diameter.

3.4 Evaluation indexes

This chapter proposes four indexes for evaluating a fiber bundle surface, namely, *Ra*, *Rq*, *Rsk*, and *Rku*. To illustrate how the four indexes can estimate the main type and degree of damage of a fiber bundle surface, the side surface and end surface of C_f/SiC with processing angle of 90° are taken as a demonstration. The surfaces of C_f/SiC were process with three machining methods: a) ground using a grinding wheel with a wheel speed of 15 m/s, grinding depth of 0.15 mm, feed rate of 4 m/min, and grain mesh size of 80#; b) polished using a 1200# sandpaper under a constant force of 5 N, spindle speed of 0.1 m/s, and sliding time of 60s; and c) friction against a ZrO_2 disk under a constant force of 30 N, spindle speed of 0.5 m/s, and sliding time of 3600 s. The three different methods caused different surface topographies and damages. Therefore, a proper set of indexes should be able to reflect the difference of the six kinds of surfaces.

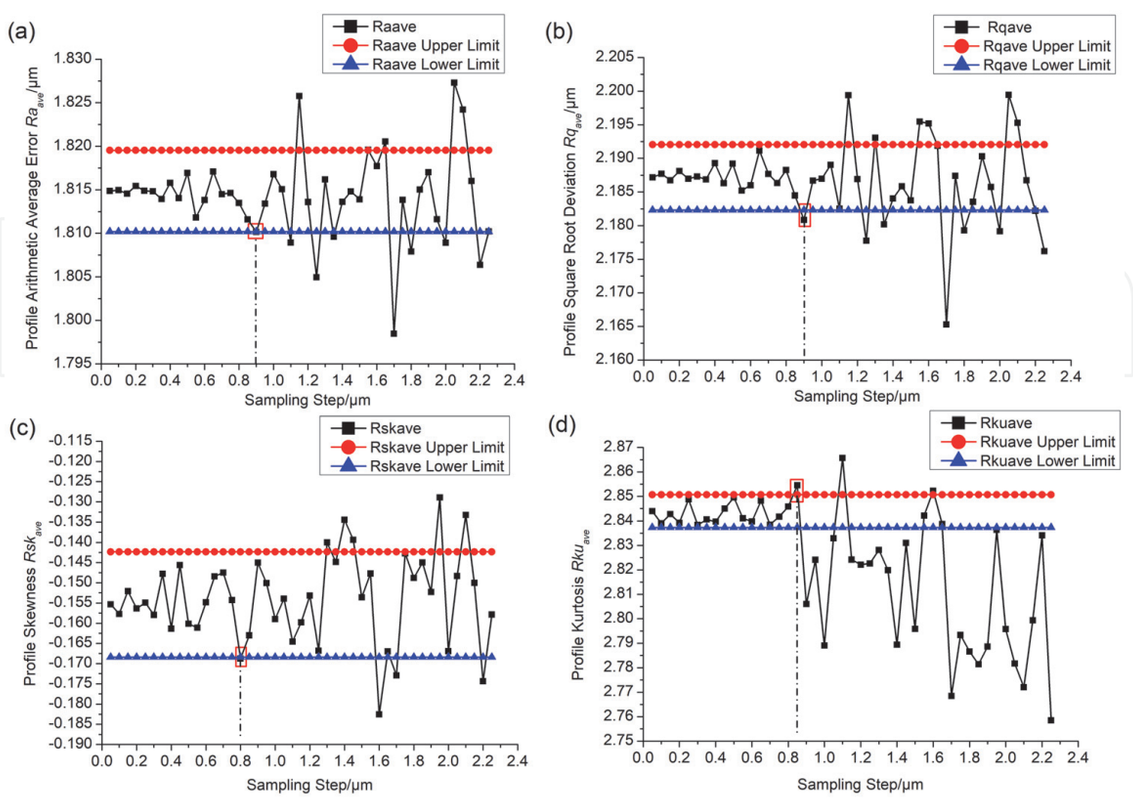

Figure 10.
Changing trends of four evaluation indexes with increasing sampling steps on fiber bundle side surface [27]. (a) Ra_{ave}, (b) Rq_{ave}, (c) Rsk_{ave}, and (d) Rku_{ave}.

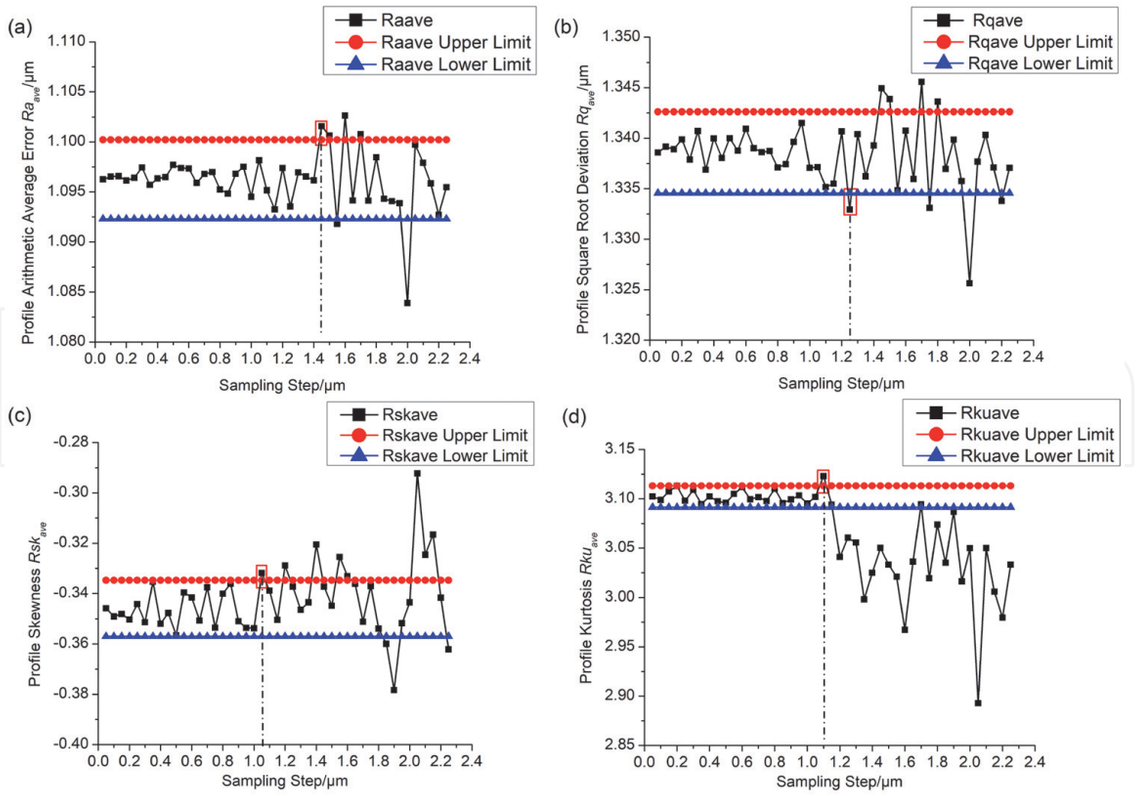

Figure 11.
Changing trends of four evaluation indexes with increasing sampling steps on fiber bundle end surface [27]. (a) Ra_{ave}, (b) Rq_{ave}, (c) Rsk_{ave}, and (d) Rku_{ave}.

Fiber bundle surface	Ra_{ave}/μm	Rq_{ave}/μm	Rsk_{ave}	Rku_{ave}
Side surface, ground	1.97 ± 0.03	2.44 ± 0.03	−0.55 ± 0.05	3.29 ± 0.10
Side surface, sandpaper polished	0.98 ± 0.02	1.41 ± 0.05	−2.15 ± 0.09	6.48 ± 0.59
Side surface, friction	0.56 ± 0.02	0.78 ± 0.02	−0.84 ± 0.07	7.96 ± 0.44
End surface, ground	1.23 ± 0.02	1.56 ± 0.03	−0.31 ± 0.04	3.60 ± 0.12
End surface, sandpaper polished	0.26 ± 0.01	0.36 ± 0.01	−1.39 ± 0.35	12.80 ± 0.55
End surface, friction	0.20 ± 0.01	0.24 ± 0.01	−0.34 ± 0.19	21.14 ± 2.88

Table 1.
Fiber bundle surface parameters of three processing methods [27].

After measuring the six surfaces with the sampling length of 280 μm and sampling number of 200, the scanning track perpendicular to the fiber orientation and machining direction, and the sampling step of 0.5 μm, four indexes can be calculated for every surface. The results are shown in **Table 1**.

The data in **Table 1** reflect that, regardless of the surface processing method used, the side surfaces are rougher than the end surfaces, which can be indicated by all side surfaces having larger Ra_{ave} and Rq_{ave} than the end surfaces. This phenomenon can be explained as follows. During the machining process, the anti-shear strength of the end surface is stronger; it is thus not easy for the fibers to be pulled-out and form surface damage, and the end surface becomes smoother than the side surface. However, fiber debonding and fiber delamination are more likely to appear, leading to more damage and a rougher surface on the side surface. In addition, for both fiber orientation surfaces, Ra_{ave} and Rq_{ave} of the friction-applied surfaces are the smallest, followed by sandpaper-polished surfaces, and finally

ground surfaces. A conclusion can be made that Ra_{ave} and Rq_{ave} are both valid in evaluating the degree of surface roughness. The rougher the surface is, the larger Ra_{ave} and Rq_{ave} are.

As a comparison, Rku_{ave} of either a ground side surface or a ground end surface is roughly equal to 3. That is, the height distribution approximately obeys a Gaussian distribution on both surfaces. Polishing with sandpaper or sliding against a ZrO_2 disk can make the surfaces flat, thus decreasing the amount of surface damage. Meanwhile, they show larger Rku_{ave} values. It is clear that the surfaces after friction turn out to have the fewest numbers of surface defects, and Rku_{ave} of the friction surfaces has the biggest value among the three processing methods on both the side and end surfaces. It can be seen that Rku_{ave} is related to the amount of surface damage. The less damage a surface has, the larger Rku_{ave} is.

For both ground surfaces, Rsk_{ave} is close to 0, which is consistent with their Gaussian distribution characteristic. For the surfaces polished by a sandpaper, the crests are chipped off during this processing, with the original troughs remaining, and thus it is reasonable for these two surfaces to have a larger negative Rsk_{ave}. After friction is applied, however, their Rsk_{ave} values reach closer to 0 again, which can be explained by the wear debris embedded into the troughs during the friction

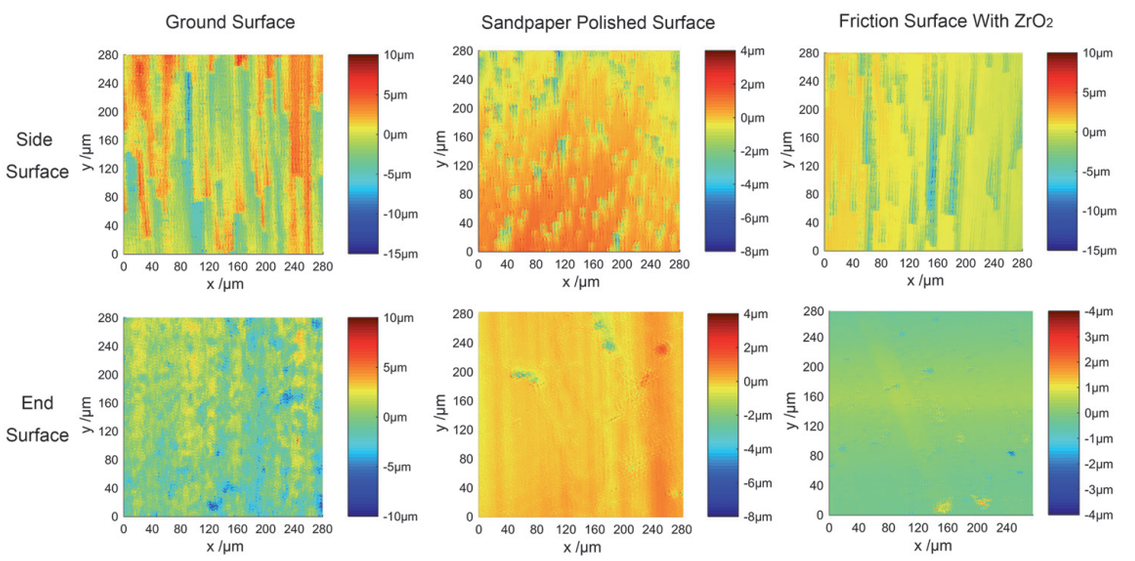

Figure 12.
Topographies of the six surfaces [27].

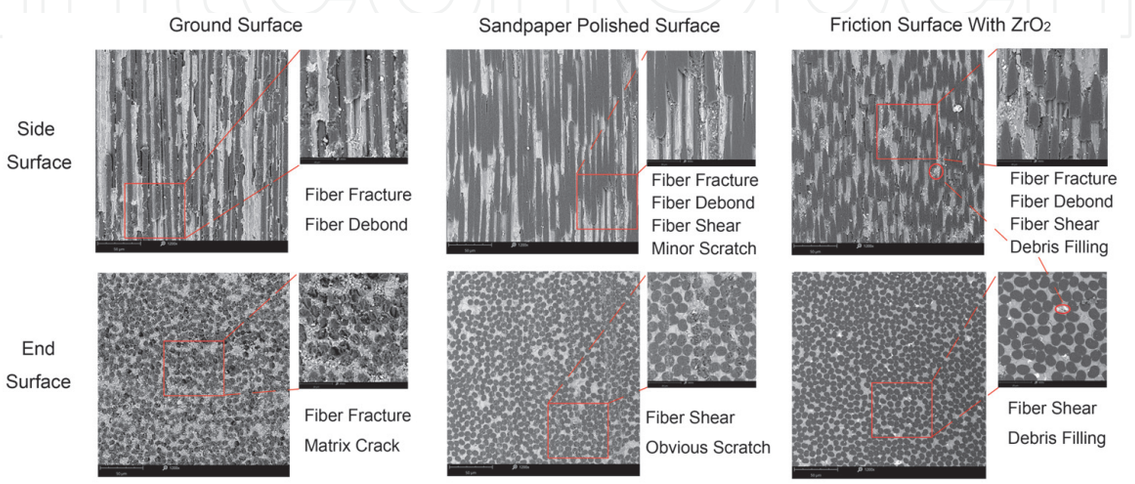

Figure 13.
SEM images of the six surfaces [27].

process decreasing the height of the troughs. Thus, it can be inferred that Rsk_{ave} is able to reflect the damage type or degree of the surface. A larger negative Rsk_{ave} value is caused by a trough-dominant surface, and a larger positive Rsk_{ave} value is caused by a crest-dominant surface. The surface state can be inferred by combining Rsk_{ave} and Rku_{ave}.

Figure 12 shows the fiber bundle surface topographies of three processing methods. **Figure 13** shows the microscopic surface topography of six surfaces. It is clear that the values of the four proposed indexes have a strong and direct connection with the surface damage and, thus, have a good feasibility and interpretability for a surface evaluation.

4. The measurement and evaluation of cell body surfaces and the whole surfaces

4.1 Measurement strategy

Cell body contains different fiber bundle orientations, and the whole surface is composed of cell bodies; thus standard procedures designated to 2D profile sampling at fiber bundle are in general not applicable for 3D topography measurement for cell body and the whole surfaces, because 2D measurement is of directionality which mainly reflects the damage between fibers, the fiber, and the matrix. Whereas for cell body and the whole surfaces, the scales are bigger, thus the measurement and evaluation mainly reflect the damage between fiber bundles and the matrix, which cannot consider the integrated effect of the fiber orientation and the processing direction simultaneously. Therefore, a 3D surface measurement and evaluation method should be adopted at these two grades.

4.2 Determination of MaxSS on cell body surfaces

A proper sampling step can make the surface information of a cell body extracted accurately and meanwhile save the cost of data collection and processing. MaxSS refers to the balance point of the accuracy and sampling cost. If a sampling step larger than the MaxSS is adopted, the information of a surface is distorted; if a sampling step larger than the MaxSS is adopted, unnecessary data sampling cost is spent. Therefore, how to determine the MaxSS on a cell body surface is very important. This section proposes a method for this topic, based on the principle of residual estimation.

For a cell body surface, the following steps can be executed to determine the MaxSS:

Sample the surface using a small sampling step of the measurement device which is at least one third of the WCMC fiber diameter.

Calculate *Sa*, *Sq*, *Ssk*, and *Sku* based on the sampling results, and set them as surface standard values θ (the standard value here does not refer to the ideal measurement result which has no error, rather, it means a standard which can be used to check whether other measurement results are acceptable).

Generally speaking, this standard value θ, containing measurement error, can be regarded as a random variable, which obeys Normal distribution, so, $\theta \sim N(\mu_1, {\sigma_1}^2)$. A measurement result $\overline{\theta}$ that is obtained from a larger sampling step obeys Normal distribution as well, so, $\overline{\theta} \sim N(\mu_2, {\sigma_2}^2)$. Because θ and $\overline{\theta}$ are both the measurement results of the same surface, their expectation is equal to the ideal real value (with no errors) of the surface. Therefore,

$$\mu_1 = \mu_2 \tag{15}$$

Set e as the difference between $\overline{\theta}$ and θ,

$$e = \overline{\theta} - \theta \tag{16}$$

Since $\overline{\theta}$ and θ are independent identically distributed (IID), their difference e obeys Normal distribution too:

$$e \sim N\left(\mu_2 - \mu_1, {\sigma_1}^2 + {\sigma_2}^2\right) \tag{17}$$

Combining Eqs. (16) and (17) together,

$$e \sim N\left(0, {\sigma_1}^2 + {\sigma_2}^2\right) \tag{18}$$

Based on the analysis above, for a set of measurement results obtained from different sampling steps, the Residual Errors (*RE*s) between each of them and the standard value θ are IID to Normal distribution, so

$$RE \sim N\left(0, \sigma^2\right) \tag{19}$$

For every actual engineering question, it is reasonable to find an acceptable range of *RE* according to the actual requirements of measurement. For example, if the ±15% smallest *RE*s are acceptable, the acceptable measurement results fall into the range of

$$[\theta\text{-}0.39\sigma, \theta + 0.39\sigma] \tag{20}$$

When the sampling step is small enough, the measurement result is in the range above. However, if the sampling step grows larger, the measurement result will go out of the range sooner or later. The largest sampling step that holds the measurement result within the range of Eq. (20) can be defined as the MaxSS for cell body surface measurement.

Here we take the measurement of a cell body of the C_f/SiC with processing angle of 90° as an example. The sampling steps of 1–45 μm were adopted to measure the cell body. The measurement results of 1 μm were set as the standard values. The rest of the results were compared with the standard values to calculate the *RE*s. The acceptable ranges of measurement results are available through Eq. (20).

The changing trends of the measurement results of the four evaluation indexes under different sampling steps are illustrated in **Figure 14**. The red and blue lines refer to the boundaries of the acceptable ranges calculated from Eq. (20). It is clear that when the sampling steps exceed a certain value (in red blocks), the corresponding results begin to go out of the ranges. Then the MaxSS can be determined for each index. Combining the four MaxSSs together, the MaxSS is available and for this material, it is 7 μm.

It can also be proved that the MaxSS of a cell body is approximately equal to the diameter of its reinforcing fiber.

4.3 Relationship between the measurement of cell body and the whole surface

The whole surface of a WCMC consists of many cell bodies. Some cell bodies nearby each other faced the same fabrication and machining process and may perform similar surface quality. Therefore, the measurement and evaluation of a

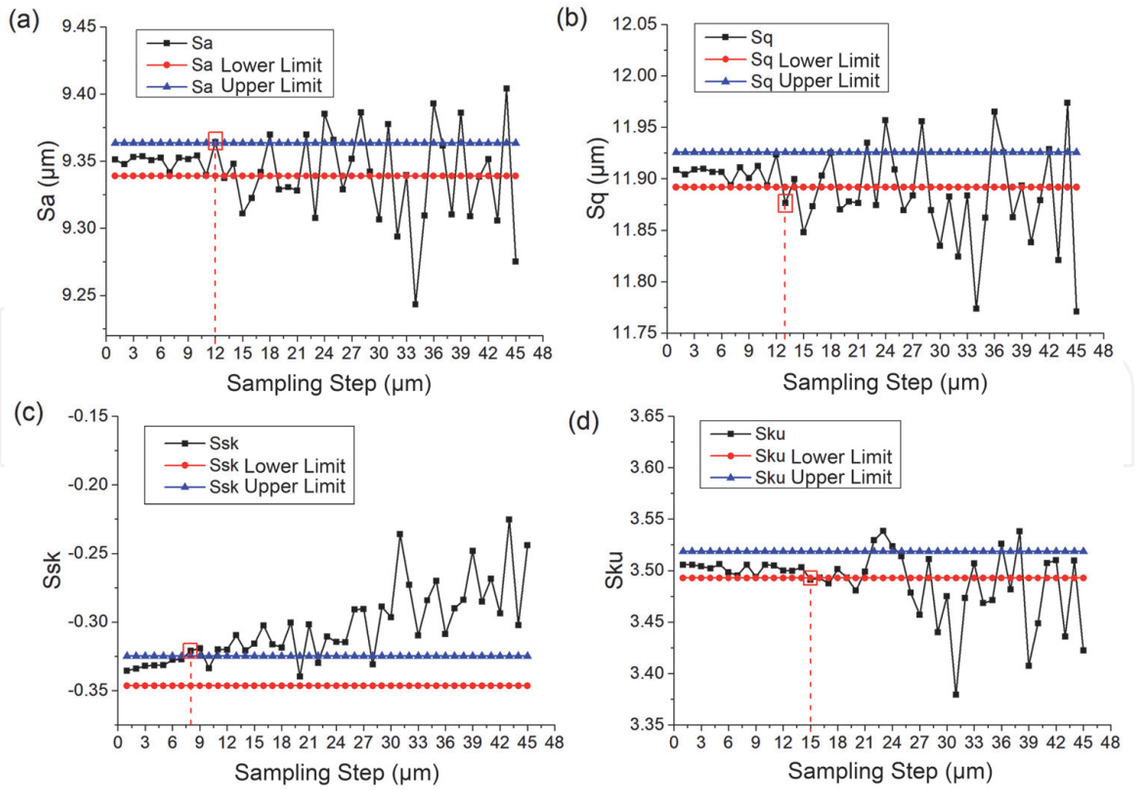

Figure 14.
The changing trends of (a) Sa (b) Sq (c) Ssk and (d) Sku with sampling steps on cell body surface [28].

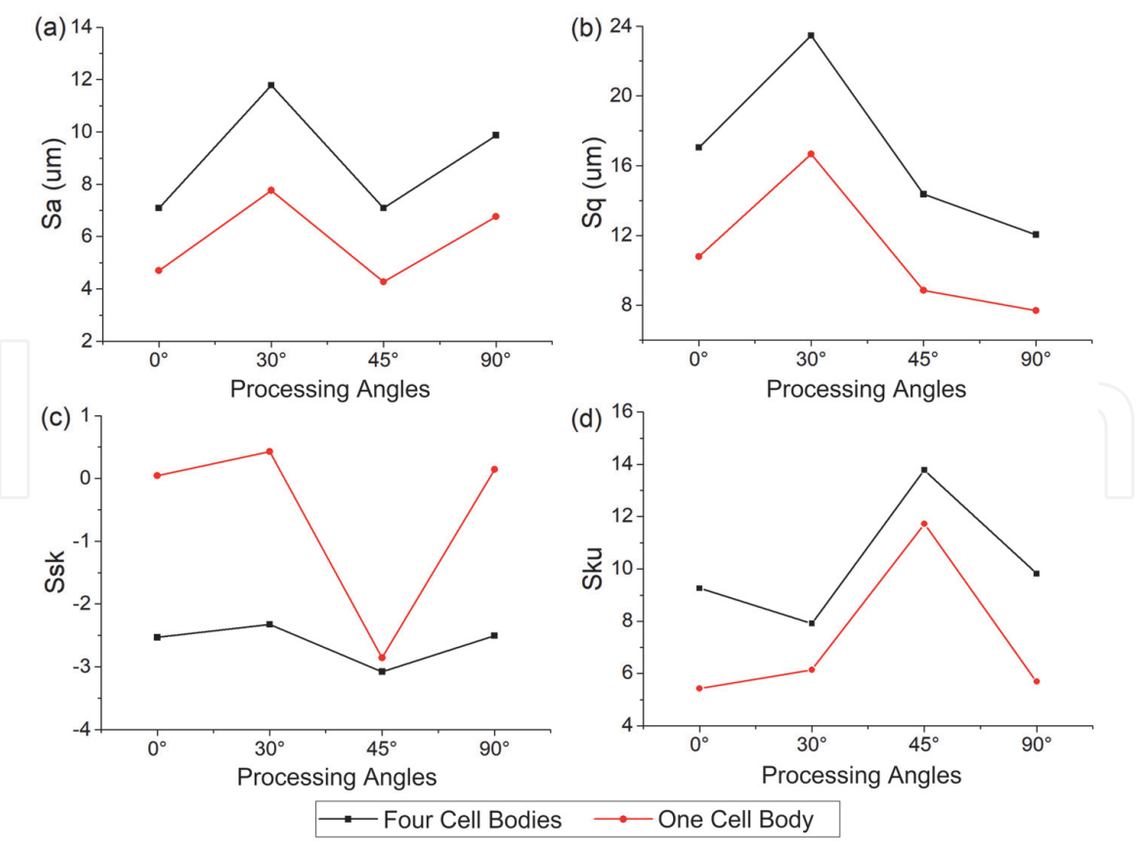

Figure 15.
Evaluation parameters with processing angles on cell body surface of C_f/SiC (a) Sa, (b) Sq, (c) Ssk, and (d) Sku.

cell body can be used to estimate the surface quality state of a certain area nearby it. It has been proved that, for the exampled C_f/SiC with processing angles of 0°, 30°, 45°, and 90°, the measurement results of the four indexes of one cell body have the similar values with the results of the nearby four cell bodies (shown in **Figure 15**).

5. Conclusions

This chapter aims at providing a grading surface measurement and evaluation system for woven ceramic matrix composites. The system contains four grading of fiber, fiber bundle, cell body, and the whole surface. The main conclusions are as follows:

1. The type and degree of the damage on fibers influence the processing quality and property of the surface. The diameter and the direction of the fibers determine the measurement parameters when sampling fiber bundle or cell body surfaces.

2. 2D measurement should be adopted on fiber bundle surfaces. Sampling parameters, including sampling length, number, step, and direction should be determined carefully to balance the accuracy and the efficiency. Four evaluation indexes, namely, *Ra*, *Rq*, *Rsk*, and *Rku*, are usable for fiber bundle surface evaluation.

3. 3D measurement should be adopted on cell body surfaces. Maximum sampling step can be determined with the principle of residual estimate. *Sa*, S*q*, *Ssk*, and *Sku* are usable on this grade.

4. The whole surface is consist of many cell bodies. Therefore, a small number of cell bodies can be used to represent a larger area nearby. This idea can help reduce the workload when measuring and evaluating a large area of WCMC surface.

Acknowledgements

Special thanks the National Natural Science Foundation of China (Nos. 51375333 and 51805366) for financial assistance.

Conflict of interest

All the authors listed have approved the manuscript, and no interest of any third parties is infringed.

Author details

Bin Lin*, Haoji Wang and Jinhua Wei
Key Laboratory of Advanced Ceramics and Machining Technology of Ministry of Education, Tianjin, China

*Address all correspondence to: linbin@tju.edu.cn

References

[1] Söderfjäll M, Herbst HM, Larsson R, Almqvist A. Influence on friction from piston ring design, cylinder liner roughness and lubricant properties. Tribology International. 2017;**116**: 272-284

[2] Erol O, Powers BM, Keefe M. Effects of weave architecture and mesoscale material properties on the macroscale mechanical response of advanced woven fabrics. Composites Part A: Applied Science and Manufacturing. 2017;**101**:554-566

[3] Hosseini Monazzah A, Pouraliakbar H, Bagheri R, Seyed Reihani SM. Al-Mg-Si/SiC laminated composites: Fabrication, architectural characteristics, toughness, damage tolerance, fracture mechanisms. Composites Part B: Engineering. 2017; **125**:49-70

[4] Cao HM, Zhou X, Li XY, Lu K. Friction mechanism in the running-in stage of copper: From plastic deformation to delamination and oxidation. Tribology International. 2017;**115**:3-7

[5] Krenkel W, Heidenreich B, Renz R. C/C-SiC composites for advanced friction systems. Advanced Engineering Materials. 2002;**4**:427-436

[6] Manocha LM, Prasad G, Manocha S. Carbon-ceramic composites for friction applications. Mechanics of Advanced Materials and Structures. 2014;**21**: 172-180

[7] Sullivan P. J and blunt L, Three-dimensional characterization of indentation topography: Visual characterization. Wear. 1992;**159**: 207-221

[8] Senin N, Ziliotti M, Groppetti R. Three-dimensional surface topography segmentation through clustering. Wear. 2007;**262**:395-410

[9] Zhao F. 3D evaluation method of cutting surface topography of carbon/phenolic (C/Ph) composite. Journal of Wuhan University of Technology—Materials Science Edition. 2011;**26**: 459-463

[10] Hintze W, Cordes M, Koerkel G. Influence of weave structure on delamination when milling CFRP. Journal of Materials Processing Technology. 2015;**216**:199-205

[11] Cao X, Lin B, Wang Y, Wang S. Influence of diamond wheel grinding process on surface micro-topography and properties of SiO_2/SiO_2 composite. Applied Surface Science. 2014;**292**: 181-189

[12] Cao X, Lin B, Zhang X. Investigations on grinding process of woven ceramic matrix composite based on reinforced fiber orientations. Composites Part B: Engineering. 2015; **71**:184-192

[13] Zhao F-L, Al C-Z, Yang D-J, Yang Z-X, Wang J-M, Ao M. Study on the evaluation method and evaluation parameters of cutting surface roughness of carbon/carbon composite. Acta Metrologica Sinica. 2006;**27**:206-211

[14] Senin N, Ziliotti M, Groppetti R. Three-dimensional surface topography segmentation through clustering. Wear. 2007;**262**:395-410

[15] Hocheng H, Tai N. H and Liu C S, Assessment of ultrasonic drilling of C/SiC composite material. Composites Part A: Applied Science and Manufacturing. 2000;**31**:133-142

[16] Tashiro T, Fujiwara J, Takenaka Y. Grinding of C/C-SiC Composite in Dry Method. London: Springer; 2007

[17] Xu W, Zhang LC. On the mechanics and material removal mechanisms of

vibration-assisted cutting of unidirectional fibre-reinforced polymer composites. International Journal of Machine Tools and Manufacture. 2014; **80–81**:1-10

[18] Zhang L, Ren C, Ji C, Wang Z, Chen G. Effect of fiber orientations on surface grinding process of unidirectional C/SiC composites. Applied Surface Science. 2016;**366**: 424-431

[19] Fabre D, Bonnet C, Rech J, Mabrouki T. Optimization of surface roughness in broaching CIRP. Journal of Manufacturing Science and Technology. 2017;**18**:115-127

[20] Bian R, He N, Ding W, Liu S. A study on the tool wear of PCD micro end mills in ductile milling of ZrO_2 ceramics. The International Journal of Advanced Manufacturing Technology. 2017;**92**:2197-2206

[21] Cao X. Lin B and Zhang X, A study on grinding surface waviness of woven ceramic matrix composites. Applied Surface Science. 2013;**270**:503-512

[22] Chou T-W, Ko FK. Textile structural composites. In: Composite Materials Series. Vol. 3. Amsterdam, New York, USA: Elsevier Science Publishers; 1989

[23] Mouritz A, Baini C, Herszberg I. Mode I interlaminar fracture toughness properties of advanced textile fibreglass composites. Composites Part A: Applied Science and Manufacturing. 1999;**30**: 859-870

[24] Wei J, Lin B, Cao X, Zhang X, Fang S. Two-dimensional evaluation of 3D needled Cf/SiC composite fiber bundle surface. Applied Surface Science. 2015;**355**:166-170

[25] Fan SW, Xu YD, Zhang LT, Cheng LF, Yu L, Yuan YD, et al. Three-dimensional needled carbon/silicon carbide composites with high friction performance. Materials Science and Engineering: A. 2007;**467**:53-58

[26] Wei J, Lin B, Wang H, Sui T, Yan S, Zhao F, et al. Friction and wear characteristics of carbon fiber reinforced silicon carbide ceramic matrix (Cf/SiC) composite and zirconia (ZrO_2) ceramic under dry condition. Tribology International. 2018;**119**:45-54

[27] Wei J, Wang H, Lin B, Sui T, Wang A, Zhao F, et al. Measurement and evaluation of fiber bundle surface of long fiber reinforced woven composites. Surface Topography: Metrology and Properties. 2019;**7**:015003

[28] Wei J, Wang H, Lin B. Measurement of cell body and the whole surfaces of long fiber reinforced woven composites. In: IOP Conference Series: Materials Science and Engineering. Vol. 678. 2019. p. 012029